Monotonic convergent quantum optimal control method with exact equality constraints on the optimized control fields

Chuan-Cun Shu, Tak-San Ho, and Herschel Rabitz

Phys. Rev. A **93**, 053418 — Published 18 May 2016

DOI: 10.1103/PhysRevA.93.053418

Monotonic convergent quantum optimal control method with exact equality constraints on the optimized control fields

Chuan-Cun Shu,[1,2,*] Tak-San Ho,[1,†] and Herschel Rabitz[1,‡]

[1] *Department of Chemistry, Princeton University, Princeton, New Jersey 08544, USA*

[2] *School of Engineering and Information Technology, University of New South Wales at the Australian Defence Force Academy, Canberra, ACT 2600, Australia*

Abstract

We present a monotonic convergent quantum optimal control method that can be utilized to optimize the control field while exactly enforcing multiple equality constraints for steering quantum systems from an initial state towards desired quantum states. For illustration, special consideration is given to finding optimal control fields with (i) exact zero area and (ii) exact zero area along with constant pulse fluence. The method combined with these two types of constraints is successfully employed to maximize the state-to-state transition probability in a model vibrating diatomic molecule.

PACS numbers: 33.80.Wz, 02.60.Pn, 02.30.Yy

* c.shu@adfa.edu.au

† tsho@princeton.edu

‡ hrabitz@princeton.edu

I. INTRODUCTION

Control over the time evolution of quantum systems towards desired quantum states with tailored control fields has motivated extensive experimental and theoretical studies [1–6], ranging from the control of chemical reactions [7–11], the performance of gate transformation in quantum information systems [12], to the control in nanostructures [13] and more. While analytically accessible only in highly specialized cases [14], quantum optimal control theory (QOCT) has become a powerful tool for designing optimal control fields that can maximize the control objective [15–20]. The subject of finding reasonable control fields subject to various constraints governed by partial differential equations while maintaining monotonic convergence of the optimization algorithms is among the most challenging problems at the frontier of quantum control research [21–28]. In a recent study [29], we proposed a gradient-based frequency domain quantum optimal control method to optimize the spectral field of laser pulses subject to multiple external constraints. For the present work, we generalize this method to the time domain to directly optimize the temporal control fields while taking into account multiple equality constraints. As illustrations, the method will be performed to find optimal control fields with (i) exact zero area, and (ii) exact zero area while keeping pulse fluence constant. The time-integrated zero area field constraint for a freely propagating electromagnetic pulse is an important property for exploring coherent interaction of light with matter [30–33], and is required as a fundamental condition for satisfying the Maxwell's equations [27]. Only have there been limited attempts to take into account such constraint in the contexts of local control theory (LCT) and QOCT [27, 34]. However, these previously proposed LCT- and QOCT-based methods in principle do not exactly reduce the field area to zero and, as a result, an additional filtering process is required to accurately render a zero-area field. The constant fluence constraint on the optimized control field has been considered in our previous work by fixing the spectral amplitude of the control unchanged [29]. Here, we will apply this requirement to the full control field in the time domain. In addition, the present method can directly include these desired constraints into optimizations and guarantee monotonic convergence of the algorithm, which is fundamentally different from the brute force strategy by applying the constraints after each iteration [16].

II. THEORETICAL METHODS

We consider a closed N-level quantum system $|0\rangle, \cdots, |N-1\rangle$ governed by the time-dependent Hamiltonian $H(t) = H_0 - \mu\mathcal{E}(t)$, where H_0 is the field-free Hamiltonian with eigenenergies $\{E_n\}$, μ the dipole operator, and $\mathcal{E}(t)$ the control field of a finite pulse length T. The objective is to identify an optimal control field that maximizes the transition probability $P_{i\to f}$ for population transfer from an initial state $\mid i\rangle$ to a specified final state $\mid f\rangle$ at the final time T. The time-dependent evolution of the quantum system is described by the wave function $\psi(t) = U(t,0)\psi(0)$, where $U(t,0)$ is the corresponding unitary evolution matrix governed by the time-dependent Schrödinger equation,

$$i\hbar\frac{\partial U(t,0)}{\partial t} = H(t)U(t,0), \quad U(0,0) \equiv \mathbb{I}, \tag{1}$$

and $\psi(0)$ is the state of the quantum system at the initial time $t = 0$.

In the present method, the local gradient-based algorithm utilized to optimize the control field is a variant of D-MORPH [35, 36], in which the control field $\mathcal{E}(t)$ is parameterized by $s \geq 0$ with $\mathcal{E}(s,t)$ morphing from $\mathcal{E}(0,t)$ at $s = 0$ in steps $s \to s + ds$ (i.e., $\mathcal{E}(s,t) \to \mathcal{E}(s+ds,t)$. Without considering any constraints on the control field, maximizing $P_{i\to f}$ entails satisfying the monotonic convergence condition [37]

$$\begin{aligned} g_0(s) &\equiv \frac{dP_{i\to f}[\mathcal{E}(s,\cdot)]}{ds} \\ &= \int_0^T \frac{\delta P_{i\to f}[\mathcal{E}(s,\cdot)]}{\delta\mathcal{E}(s,t)}\frac{\partial\mathcal{E}(s,t)}{\partial s}dt \geq 0. \end{aligned} \tag{2}$$

A monotonic increase in $P_{i\to f}$ can be ensured by integrating the first-order differential equation

$$\frac{\partial\mathcal{E}(s,t)}{\partial s} = \frac{\delta P_{i\to f}[\mathcal{E}(s,\cdot)]}{\delta\mathcal{E}(s,t)}, \quad s > 0. \tag{3}$$

The unconstrained D-MORPH algorithm in Eq. (3) can be generalized to include a set of exact equality constraints on the control fields

$$h_m\left[\mathcal{E}(s,\cdot)\right] = C_m \quad m = 1, 2, \ \ldots, M, \tag{4}$$

where $C_1, \ \ldots, C_M$ are specified constants, and $M(\geq 1)$ is the number of constraints, and thus $\partial\mathcal{E}(s,t)/\partial s$ is expanded to incorporate the conditions

$$\begin{aligned} g_m(s) \equiv \frac{dh_m[\mathcal{E}(s,\cdot)]}{ds} = \int_0^T \frac{\delta h_m[\mathcal{E}(s,\cdot)]}{\delta\mathcal{E}(s,t)}\frac{\partial\mathcal{E}(s,t)}{\partial s}dt = 0, \\ m = 1, 2, \ \ldots, M, \end{aligned} \tag{5}$$

which is a manifestation of the equality constraints given in Eq. (4).

The condition Eq. (2) is satisfied when $\partial\mathcal{E}(s,t)/\partial s$ is proportional to the derivative $\delta P_{i\to f}[\mathcal{E}(\cdot)]/\delta\mathcal{E}(t)$ [35, 37], while the conditions Eq. (5) are satisfied when $\partial\mathcal{E}(s,t)/\partial s$ is orthogonal to all of the derivatives $\delta h_m/\delta\mathcal{E}$. The combined conditions Eqs. (2) and (5) can be fulfilled by expressing $\partial\mathcal{E}(s,t)/\partial s$, in a projection operator formulation, as

$$\frac{\partial\mathcal{E}(s,t)}{\partial s} = S(t)\left\{g_0(s)\sum_{\ell=0}^{M}\left[\Gamma^{-1}\right]_{0\ell}\mathcal{P}c_\ell(s,t) + (1-\mathcal{P})\beta(s,t)\right\} \tag{6}$$

where $S(t)\geq 0$ is the pulse profile that smoothly switches the control field on and off, $\beta(s,t)$ is an arbitrary function, implying that there exist multiple solutions to Eqs. (2) and (5), and the coefficients $c_\ell(s,t)$ are defined as

$$c_\ell(s,t) = \begin{cases} \dfrac{\delta P_{i\to f}[\mathcal{E}(s,t)]}{\delta\mathcal{E}(s,t)}, & \ell = 0 \quad (7a) \\ \dfrac{\delta h_\ell[\mathcal{E}(s,t)]}{\delta\mathcal{E}(s,t)}, & \ell = 1,...,M. \quad (7b) \end{cases}$$

The $M+1$ dimensional symmetric square matrix Γ in Eq. (6) is composed of elements

$$\Gamma_{\ell\ell'} = \int_0^T S(t)c_\ell(s,t)c_{\ell'}(s,t)dt. \tag{8}$$

Here the matrix Γ is assumed to invertible (i.e., full rank). For large values of M, regularization may be needed to compute the corresponding inverse matrix Γ^{-1} [38]. The action of the projection operator $\mathcal{P}$ on an arbitrary function $\alpha(s,t)$ is given by

$$\mathcal{P}\alpha(s,t) \equiv \int_0^T S(t')\left(\sum_{k,k'=0}^{M} c_k(s,t)\left[\Gamma^{-1}\right]_{kk'}c_{k'}(s,t')\right)\alpha(s,t')dt' \tag{9}$$

.

By inserting Eq. (6) into Eqs. (2) and (5), we can verify that

$$\begin{aligned} g_{\ell'} &= g_0(s)\int_0^T S(t)c_{\ell'}(s,t)\sum_{\ell=0}^{M}\left[\Gamma^{-1}\right]_{0\ell}\mathcal{P}c_\ell(s,t)dt + \int_0^T S(t)c_{\ell'}(s,t)t)\left(1-\mathcal{P}\right)\beta(s,t)dt \\ &= g_0(s)\delta_{0\ell'} + \int_0^T S(t)c_{\ell'}(s,t)\beta(s,t)dt - \sum_{k'=0}^{M}\delta_{\ell' k'}\int_0^T S(t')c_{k'}(s,t')\beta(s,t')dt' \\ &= g_0(s)\delta_{0\ell'} \qquad \ell' = 0,1,...,M. \end{aligned} \tag{10}$$

is always greater than ($\ell' = 0$) or equal ($\ell' \neq 0$) to zero, indicating that Eq. (6) satisfies the criteria set out in Eqs. (2) and (5) for any choice of $\beta(s,t)$. The initial-value differential equation Eq. (6) is integrated starting from an initial control field $\mathcal{E}(0,t)$, until an optimal control $\mathcal{E}(s_\infty,t)$ is obtained at $s = s_\infty$ such that the control objective $P_{if}(T)$ is maximized. With reasonably imposed equality constraints, the objective may still approach its global maximum value $P_{i\to f} = 1.0$. However, strongly demanding and competing constraints may result in a suboptimal solution $P_{i\to f} < 1.0$, even at the best attainable control field.

In the remainder of the paper, we will set $\beta(s,t) = 0$ to show the basic principles of the procedure, and thus Eq. (6) becomes

$$\frac{\partial \mathcal{E}(s,t)}{\partial s} = S(t) g_0(s) \sum_{\ell=0}^{M} \left[\Gamma^{-1}\right]_{0\ell} c_\ell(s,t). \tag{11}$$

The gradient of $P_{i\to f}$ with respect to $\mathcal{E}(s,t)$ can thus be written as

$$\frac{\delta P_{i\to f}}{\delta \mathcal{E}(s,t)} = -2\mathrm{Im}\left\{\mathrm{Tr}\left\{[|i\rangle\langle i|, O(T)]\,\mu(t)\right\}\right\} \tag{12}$$

with $\mu(t) = U^\dagger(t,0)\mu U(t,0)$ and $O(T) = U^\dagger(T,0)|f\rangle\langle f|U(T,0)$, and it can be readily computed upon solving Eq. (1) with the control field $\mathcal{E}(s,t)$. The equality-constraint-preserving differential equation Eq. (11) is solved to morph the control field $\mathcal{E}(s,t)$ over s, starting with an initial field $\mathcal{E}(0,t)$, until the control objective $P_{i\to f}$ is maximized to an acceptable precision.

As an illustration, we desire to find pure ac optimal controls of zero area that may also preserve the control field fluence. For the pure ac control, the pulse area is zero, i.e.,

$$h_1[\mathcal{E}(s,\cdot)] = \int_0^T \mathcal{E}(s,t)dt = 0, \tag{13}$$

leading to $c_1(s,t) = 1$, whereas for the constant pulse fluence, we have

$$h_2[\mathcal{E}(s,\cdot)] = \int_0^T \mathcal{E}^2(s,t)dt = \text{constant}, \tag{14}$$

leading to $c_2(s,t) = 2\mathcal{E}(s,t)$. Reliably solving Eq. (11) coupled to the time-dependent Schrödinger Equation (1) is essential for obtaining optimal control fields. In our simulations, Eq. (11) is solved by using MATLAB routine ode45 [40], a fourth-order Runge-Kutta integrator, with a variable step size ds to determine the control field $\mathcal{E}(s,t)$, starting at $s = 0$. We remark that in principle, the initial guess field $\mathcal{E}(0,t)$ can be an aribitrary function, and we may start with a zero initial field $\mathcal{E}(0,t) = 0$, then bring the field fluence

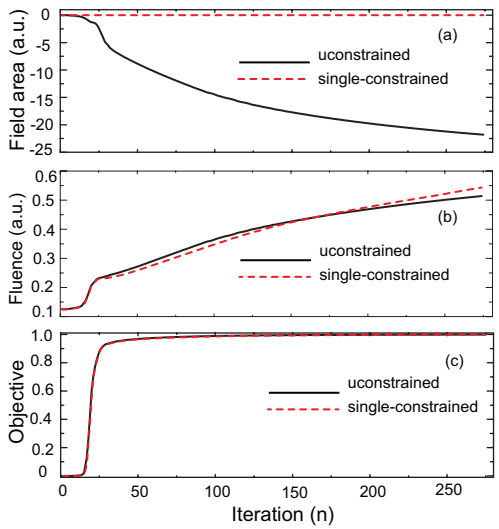

FIG. 1. The pulse area (a), fluence (b) and control objective (c) as a function of iteration for both the unconstrained and the single-constrained simulations. The result at the 0th iteration arises from the pulse $\mathcal{E}(0,t)$. Both unconstrained and constrained optimizations were stopped at $P_{i\to f} = 0.999$.

up to the intended value using the unconstrained D-MORPH method [35, 36]. However, the purpose of the following simulations is to demonstrate the utility of the proposed constrained D-MORPH method for optimizing the control field subject to the zero-area and the constant non-zero fluence equality constraints, Eqs. (13) and (14), throughout the optimization in the time domain.

III. RESULTS AND DISCUSSION

We have carried out numerical simulations for control of state-to-state transitions for a 5−level LiH molecular system composed of the five lowest vibrational levels in the ground electronic state. The energies of these five levels are $E_0 = 697.96$, $E_1 = 2057.71$, $E_2 = 3372.57$, $E_3 = 4643.45$ and $E_4 = 5871.22$ cm^{-1}. The dipole matrix elements $\mu_{\nu\nu'} = \langle \nu \mid \mu \mid \nu' \rangle$, $\nu, \nu' = 0, 1, 2, 3, 4$, are obtained from the data in Ref. [41]. We consider the vibrational ground state $|0\rangle$ as the initial state $|i\rangle$, and the target state $|f\rangle$ is a superposition state $1/\sqrt{2}(|\ 2\rangle - |\ 3\rangle)$. The convergence criterion is $P_{i\to f} > 0.999$ to ensure that the final two vibrational states $|2\rangle$ and $|3\rangle$ are equally populated. To satisfy the zero area condition in

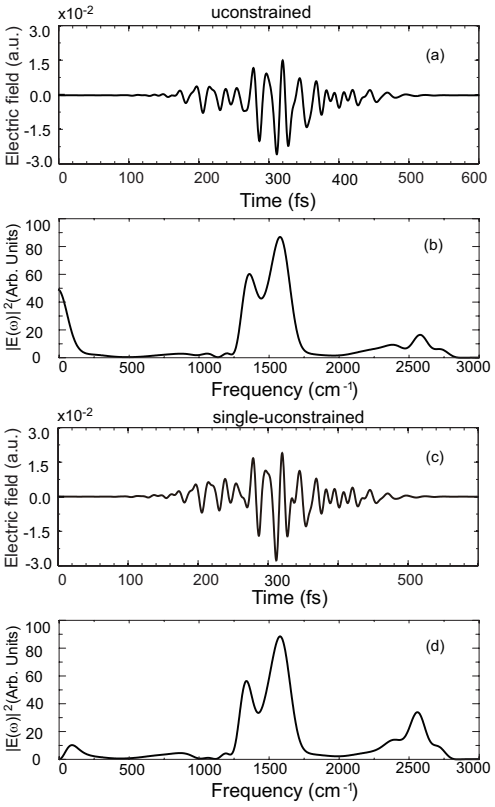

FIG. 2. The final control field and the corresponding Fourier power spectrum for the unconstrained ((a) and (b)) and ac field single-constrained ((c) and (d)) simulations.

Eq. (13) at $s = 0$, the initial control field $\mathcal{E}(0,t)$ is written as

$$\mathcal{E}(0,t) = \mathcal{E}_0 \left[\epsilon(t) - \frac{1}{T} \int_0^T \epsilon(t) dt \right], \tag{15}$$

where $\mathcal{E}_0$ denotes the control field amplitude, and in this work we choose a transform-limited laser field $\epsilon(t) = S(t)\cos[\omega_0(t-t_0)]$ with $\omega_0 = 1600$ cm^{-1}, and $t_0 = T/2 = 300$ fs. The profile $S(t) = \exp[-4\ln 2(t-t_0)^2/\tau^2]$ has a full-width at half-maximum (FWHM) $\tau = 150$ fs (bandwidth (FWHM) of 196 cm^{-1}). The field amplitude $\mathcal{E}_0$ is chosen such that the initial fluence is $\int_0^T \mathcal{E}^2(0,t)dt = 0.125$. The temporal grid was discretized with 2048 uniform time steps.

We first consider the single-constraint case of finding a zero area control field. Figure 1 plots the pulse area (i.e., the dc component), the fluence of the final control field, and the objective yield as a function of search effort (iteration) for the unconstrained and the zero area field single-constrained control simulations. Figure 1 (a) shows that the pulse area increases in magnitude with iteration when the zero area constraint is *not* imposed. As seen

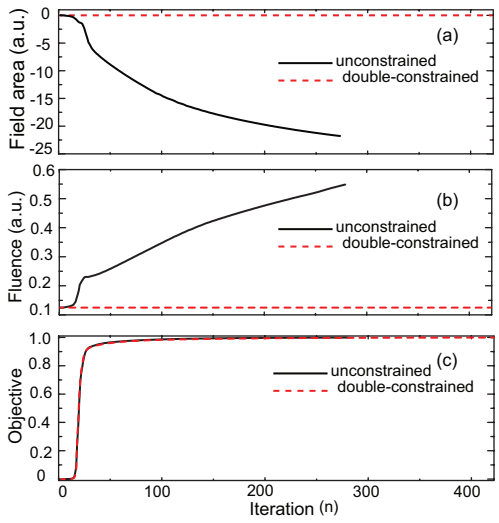

FIG. 3. The pulse area (a), fluence (b) and control objective (c) as a function of iteration for both the unconstrained and the double-constrained simulations. Both unconstrained and constrained optimizations were stopped at $P_{i\to f} = 0.999$.

from Fig. 1 (b), the fluence of the optimized pulses in both cases increases. Figure 1 (c) shows the monotonic convergence for the algorithm, which can be proved from Eq. (2). In the present simulation, imposing the zero area constraint does not affect the convergence rate, and the yield of $P_{i\to f} = 0.999$ is successfully achieved for both unconstrained and constrained cases.

Figure 2 shows the final time-dependent control fields and the corresponding Fourier power spectra $|E(\omega)|^2$ for the unconstrained and the zero area single-constrained optimal control simulations. The power spectrum beyond 3000 cm^{-1} is of little importance, because the corresponding transition dipole moment, i. e., $\mu_{03} = 7.76 \times 10^{-5}$ a.u. for transitions $|0\rangle \to |3\rangle$ with transition frequency $\hbar\omega_{03} = E_3 - E_0 = 3945$ cm^{-1}, is much smaller than the dominant ones $\mu_{01} = 0.9422\times10^{-1}$ and $\mu_{02} = 6.945\times10^{-3}$ [41] with the transition frequencies equal to $\sim$ 1360 cm^{-1} and $\sim$ 2600 cm^{-1}, respectively. The unconstrained final control field in Fig. 2 (a) clearly shows asymmetric oscillations about $\mathcal{E} = 0$ with substantially larger negative amplitudes, and the corresponding power spectrum in Fig. 2 (b) contains a pronounced dc component, in agreement with the results in Fig. 1 (a). On the other hand, the subtle shift in the asymmetry for the zero area constrained final control field in Fig. 2 (c) consists of balanced positive and negative amplitudes, and the corresponding power spectrum in Fig. 2 (d) has no dc component (as a result of a non-zero area). Both power

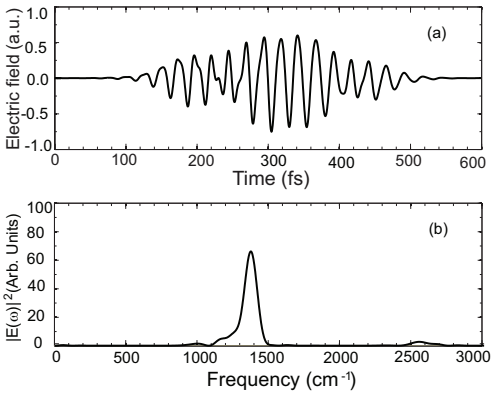

FIG. 4. (a) the optimal control field, and (b) corresponding power spectrum for the double constraints of zero area field and fixed fluence constrained simulations.

spectra in Figs. 2 (b) and (d) are extremely broadband. Specifically, it was found in both cases that the resultant optimal controls have two dominant transition frequencies, one at $\sim$ 1360 cm^{-1} corresponding to the $|0\rangle \rightarrow |1\rangle$ transition, and the other at $\sim$ 2600 cm^{-1} corresponding to the $|0\rangle \rightarrow |2\rangle$ and $|1\rangle \rightarrow |3\rangle$ transitions. This circumstance suggests the presence of two constructively interfering pathways, $|0\rangle \rightarrow |2\rangle$ and $|0\rangle \rightarrow |1\rangle \rightarrow |3\rangle$ leading to the objective state $1/\sqrt{2}(|\ 2\rangle - |\ 3\rangle)$. The peak at 1600 cm^{-1} found in the optimal fields comes from the initial field and does not correspond to any existing transitions or their combinations and may be suppressed by including further constraints on the control field. The latter situation is demonstrated below by adding the constant pulse fluence constraint described in Eq. (14). Finally, the frequency-domain constrained D-MORPH scheme [29] may be solved in conjunction with the present time-domain constrained D-MORPH one for removing the frequency components below $\sim$ 1000 cm^{-1} and above $\sim$ 2000 cm^{-1}.

We now consider the double-constrained case of finding an optimal zero area control field, while keeping the control field fluence constant. Figures 3 (a) and (b) respectively give the pulse area and fluence as a function of iteration for both unconstrained and double constrained simulations, showing that both constraints are satisfied by removing the dc component while keeping the fluence of the control field constant. Figure 3 (c) demonstrates that despite the strict double constraints, monotonic convergence to the optimal yield is preserved.

Figure 4 shows the final optimized control field and corresponding power spectrum. The control field in Fig. 4 (a) oscillates nearly symmetrically about zero. The power spectrum

in Fig. 4 (b) consists of a main peak around 1350 cm^{-1} with a broadband width of 400 cm^{-1}, which can cover all transition frequencies between neighboring vibrational states, and a very small peak around 2600 cm^{-1}, which corresponds to the direct transition frequencies $\hbar\omega_{02} = E_2 - E_0 = 2675$ cm^{-1} and $\hbar\omega_{13} = E_3 - E_1 = 2586$ cm^{-1}. Interestingly, the highest peak at 1600cm^{-1} in Figs. 2 (b) and (d) is virtually absent in Fig. 4 (b), showing that including the fluence equality constraint further restricts the available control search space. The negligible contributions from both low and high frequencies in Fig. 4 (b) does not imply that the inclusion of the fluence constraint can generally serve to filter the spectrum of control field. Additional control simulations (not shown) have been carried out using initial control fields with higher fluence and it was found that the peak around 2600 cm^{-1} was further reduced, suggesting that at the larger field fluence the corresponding optimal control pathways only involve single photon transitions between the immediate neighboring levels. The final power spectrum depends not only on the Hamiltonian H_0 of the quantum system, but also on the initial field $\mathcal{E}(0,t)$ guess. For example, by varying the frequency as well as the fluence of the initial field, the frequency distribution of the optimized control field will be changed, indicating that there exist multiple transition pathways.

In practice, the dc component along with other unwanted frequencies can also be removed by adding a spectral constraint, e.g., a bandpass filter throughout the optimization [8–10], or more systematically, using a hybrid time-frequency D-MORPH scheme that solves simultaneously the current time-domain constrained D-MORPH scheme and its frequency-domain counterpart recently formulated [29].

IV. CONCLUSION

In summary, we have presented a monotonically convergent quantum optimal control procedure for driving quantum systems towards desired control objective while talking into account multiple functional equality constraints on the control fields. As illustrations, special consideration is given to finding optimal control fields with (i) exact zero area and (ii) exact zero area along with a constant fluence. With these constraints, we performed QOCT simulations to maximize the vibrational state-to-state transition probability of the diatomic molecule LiH in the ground electronic state. It is found that the optimal yield of the target state can be successfully attained despite the additional constraints on the control field. The

framework presented in this work is amenable to general quantum control optimal problems subject to an arbitrary number of equality constraints in both the time and frequency domains, either separately or simultaneously, and may have potential applications in quantum physics including quantum information science [15].

ACKNOWLEDGMENTS

This work by C.C.S. was partially supported by the Department of Energy (USA) under Grant No. DE-FG02- 02ER15344. T.S.H. and H.R. acknowledge partial support by the National Science Foundation (USA) under Grant No. CHE-0718610. C.C.S also acknowledges partial support by the UNSW Vice-Chancellors Postdoctoral Research Fellowship (Australia).

---

[1] T. Brixner, N. H. Damrauer, P. Niklaus, and G. Gerber, Nature **414**, 57 (2001).

[2] X. H Xie, S. Roither, M. Schöffler, E. Lötstedt, D. Kartashov, L. Zhang, G. G. Paulus, A. Iwasaki, A. Baltuška, K. Yamanouchi, and M. Kitzler, Phys. Rev. X **4**, 021005 (2014).

[3] H. Rabitz, R. de Vivie-Riedle, M. Motzkus, and K. Kompa, Science **288**, 824 (2000).

[4] P. Nuernberger, D. Wolpert, H. Weiss, and G. Gerber, Proc. Natl. Acad. Sci. **107**, 10366 (2010).

[5] R. Hildner, D. Brinks, J. B. Nieder, R. J. Cogdell, and N. F. van Hulst, Science **340**, 1448 (2013).

[6] G. D. Fuchs, G. Burkard, P. V. Klimov, and D. D. Awschalom, Nat. Phys. **7**, 789 (2011).

[7] I. R. Sola, V. S. Malinovsky, and D. J. Tannor, Phys. Rev. A **60**, 3081 (1999).

[8] M. Artamonov, T.-S. Ho, and H. Rabitz, Chem. Phys. **305**, 213 (2004).

[9] M. Artamonov, T.-S. Ho, and H. Rabitz, J. Chem. Phys. **124**, 064306 (2006).

[10] Y. Kurosaki, M. Artamonov, T-S. Ho, and H. Rabitz, J. Chem. Phys. **131**, 044306 (2009).

[11] C.-C. Shu, T. Rozgonyi, L. González, and N. E. Henriksen, J. Chem. Phys. **136**, 174303 (2012).

[12] C. M. Tesch and R. de Vivie-Riedle, Phys. Rev. Lett. **89**, 157901 (2002).

[13] J. Giidde, M. Rohleder, T. Meier, S. W. Koch, and U. Hofer, Science **318**, 1287 (2007).

[14] N. Dudovich, B. Dayan, S. M. Gallagher Faeder, and Y. Silberberg, Phys. Rev. Lett. **86**, 47 (2001).

[15] S. J. Glaser, U. Boscain, T. Calarco, C. P. Koch, W. Köckenberger, Ronnie Kosloff, I. Kuprov, B. Luy, S. Schirmer, T. Schulte-Herbrüggen, D. Sugny, and . K. Wilhelm, Eur. Phys. D **69**, 279 (2015).

[16] J. Werschnik and E. K. U. Gross, J. Phys. B **40**, R175 (2007).

[17] C. Brif, R. Chakrabarti, and H. Rabitz, New J. Phys. **12**, 075008 (2010).

[18] R. Eitan, M. Mundt, and D. J. Tannor, Phys. Rev. A **83**, 053426 (2011).

[19] C.-C. Shu and N. E. Henriksen, J. Chem. Phys. **136**, 044303 (2012).

[20] C.-C. Shu, M. Edwalds, A. Shabani, T.-S Ho and H. Rabitz, Phys. Chem. Chem. Phys. **17**, 18621 (2015).

[21] I. Schaefer and R. Kosloff , Phys. Rev. A **86**, 063417 (2012).

[22] C. Gollub, M. Kowalewski, and R. de Vivie-Riedle, Phys. Rev. Lett. **101**, 073002 (2008).

[23] M. Lapert, R. Tehini, G. Turinici, and D. Sugny, Phys. Rev. A **79**, 063411 (2009).

[24] J. P. Palao, D. M. Reich, and C. P. Koch, Phys. Rev. A **88**, 053409 (2013).

[25] P. von den Hoff, S. Thallmair, M. Kowalewski, R. Siemering, and R. de Vivie-Riedle, Phys. Chem. Chem. Phys. **14**, 14460 (2012).

[26] Daniel M. Reich, José, P. Palao, and C. P. Koch, J. Mod. Opt. **61**, 822 (2014).

[27] D. Sugny, S. Vranckx, M. Ndong, N. Vaeck, O. Atabek, and M. Desouter-Lecomte, Phys. Rev. A **90**, 053404 (2014).

[28] A. Donovan, V. Beltrani, and H. Rabitz, Chem. Phys. **425**, 46 (2013).

[29] C.-C. Shu, T.-S. Ho, X. Xing, and H. Rabitz, Phys. Rev. A **93**, 033417 (2016).

[30] J. Orstigoso, J. Chem. Phys. **137**, 044303 (2012).

[31] M. Yoshida and Y. Ohtsuki, Phys. Rev. A **90**, 013415 (2014).

[32] L. S. Costanzo, A. S. Coelho, D. Pellegrino, M. S. Mendes, L. Acioli, K. N. Cassemiro, D. Felinto, A. Zavatta, and M. Bellini, Phys. Rev. Lett. **116**, 023602 (2016).

[33] H. G. Lee, Y. Song, H. Kim, H. Jo, and J. Ahn, Phys. Rev. A **93**, 023423 (2016).

[34] D. Sugny, S. Vranckx, M. Ndong, O. Atabek, and M. Desouter-Lecomte, J. Mod. Opt. **61**, 816 (2014).

[35] A. Rothman, T.-S. Ho, and H. Rabitz, J. Chem. Phys. **123**, 134104 (2005).

[36] A. Rothman, T.-S. Ho, and H. Rabitz, Phys. Rev. A **72**, 023416 (2005).

[37] K. W. Moore and H. Rabitz, Phys. Rev. A **84**, 012109 (2011).

[38] W. H. Press, S. A. Teukolsky, W. T. Vetterling, B. P. Flannery, *Numerical Recipes* (Cambridge Univeristy, 1996).

[39] H. Rabitz, T.-S. Ho, M. Hsieh, R. Kosut, and M. Demiralp, Phys. Rev. A **74**, 012721 (2006).

[40] MathWorks, MATLAB, The MathWorks, Natick, MA, 1994. (2005).

[41] B. K. Lee, J. M. Stout, and C. E. Dykstra, J. Mol. Struct. (Theochem) **400**, 57 (1997).